Study of Mechanical Behaviour of Polycrystalline Materials at the Mesoscale Using High Energy X-Ray Diffraction

Andrzej Baczmański, Elżbieta Gadalińska, Sebastian Wroński, Chedly Braham, Wilfrid Seiler, Manuel François, Léa Le Joncour, Benoît Panicaud, Thomas Buslaps, Houda Yahyaoui, et al.

Study of mechanical behaviour of polycrystalline materials at the mesoscale using high energy X-ray diffraction

Andrzej Baczmański[1, a *], Elżbieta Gadalińska[2,b], Sebastian Wroński[1,a],
Chedly Braham[3,d] Wilfrid Seiler[3,e], Manuel François[4,f], Léa Le Joncour[4,g],
Benoit Panicaud[4,h], Thomas Buslaps[5,i], Houda Yahyaoui[6,j],
Habib Sidhom[6,k] and Yuchen Zhao[4,l]

[1]AGH University of Science and Technology, WFIS, al. Mickiewicza 30, 30-059 Kraków, Poland

[2]Institute of Aviation, NET Institute, al. Krakowska 110/114, 02-256 Warszawa, Poland

[3] Arts et Métiers-ParisTech, PIMM, CNRS UMR 8006, 151 Bd de l'Hôpital, 75013 Paris, France

[4]Université de Technologie de Troyes (UTT), 12 rue Marie Curie, 10010 Troyes, France

[5]ESRF, 6, rue J. Horowitz, 38500 Grenoble Cedex, France

[6]Mechanical, Materials and Processes Laboratory (LR99ES05), ESSTT, 5, Avenue Taha Hussein 1008, University of Tunis, Tunisia

[*a]andrzej.baczmanski@fis.agh.edu.pl, [b]elzbieta.gadalinska@ilot.edu.pl,
[c]sebastian.wronski@fis.agh.edu.pl, [d]chedly.braham@paris.ensam.fr,
[e]wilfrid.seiler@paris.ensam.fr, [f]manuel.francois@utt.fr, [g]lea.le_joncour@utt.fr,
[h]benoit.panicaud@utt.fr, [i]buslaps@esrf.fr, [j]houda.yahyaoui@yahoo.fr, [k]habib.sidhom@gmail.com,
[l]yuchen.zhao@utt.fr

Keywords: X-ray diffraction, synchrotron radiation, multiscale modelling, strain measurement, plastic deformation

Abstract. Owing to its selectivity, diffraction is a powerful tool for analysing the mechanical behaviour of polycrystalline materials at the mesoscale, i.e. phase and grain scale. "In situ" synchrotron diffraction (transmission mode) during tensile tests and modified self-consistent elastoplastic model were used to study elastic and plastic phenomena occurring in polycrystalline specimens during deformation. The evolution of stress for grains which belong to different phases of duplex stainless steel and pearlitic steel was analyzed.

Introduction

Multi-scale crystallographic models are very convenient for the study of elastoplastic properties in microscopic and macroscopic scales. Comparison of experimental data with model predictions allows us to understand the physical phenomena occurring during sample deformation at the level of crystallites in polycrystalline/multiphase materials [1-6]. Moreover, the micro and macro parameters of elastoplastic deformation can be experimentally established. In our previous works the interpretation of diffraction results was based on a self-consistent crystallographic model of elastoplastic deformation providing reliable statistical information about grain/phase behaviour in polycrystalline specimens [4-6]. This model was previously applied to predict interactions between grains (and phases) during elastic – plastic transition of the deformed samples. Model results have been successfully verified on duplex stainless steel samples using diffraction data [4-6]. In the present work the lattice strain evolution in both phases of two two-phases steels, pearlitic and duplex, are measured "in situ" during tensile test by using high energy X-ray diffraction.

Experiment

The pearlitic steel EN C70 (SAE 1070), studied in this work, was provided by ASCOMETAL French company in the form of cylindrical bars of 80 mm in diameter obtained by hot rolling. The

chemical composition of this steel is given in Table 1. The C70 pearlitic steel was obtained by austenization at 1323 K for 0.11 h followed by cooling under blowing air. The microstructure of so obtained steel is shown in Fig.1a.

The second material studied is an duplex stainless steel (UR45N), containing approximately 50% austenite and 50% ferrite, obtained by continuous casting and then hot rolled down to a 15 mm sheet thickness. The chemical composition of the material is given in Table 1 (influence of chemical composition on phases hardness were studied in [5]).The samples from UR45N steel were annealed during 1 000 hours at a temperature of 673 K and then cooled in air. Such thermal treatment cause significant increase hardness of ferrite, while hardness of austenite remains unchanged (details of phase transformation are given in [6]). The characteristic microstructure of the studied steel consists of austenitic islands elongated along the rolling direction and embedded in a ferritic matrix (see Fig. 1b and [6]).

Measurements. Combined X-ray diffraction and in situ tensile tests were performed at the ID15B beamline (ESRF, Grenoble, France) applying monochromatic X-ray radiation (wavelength $\lambda = 0.14256$ Å) with a beam size of 100 x100 μm^2 in transmission mode (average through the sample thickness). In order to determine lattice strains diffraction patterns were recorded in the range $2\theta= 1.8° – 7°$ with a 2D detector (Thales, Pixium 4700 [7]) covering the main reflections from steel.

For the uniaxial *in situ* tensile loading tests a hydraulic 5kN rig was used and "dog bone" shaped samples of suitable dimensions (1.5 x 1.5 mm^2 cross section) were studied. The load was applied along RD (rolling direction) in load control mode with a load rate equal to 1 N/s (i.e. 0.44 MPa/s for the stress rate). Diffraction data were collected with exposure time equal to 10 s separated by 5 s intervals without acquisition. The sample strain was monitored by the position of the hydraulic actuator. Macroscopic stress-strain plots are presented in Fig. 2 for both materials. The inter-planar spacings $< d >_{\{hkl\}}$ were determined using the FIT2D [8] and MULTIFIT [9] software. The first program enables conversion of 2D images obtained by the PIXIUM detector into one dimensional 2θ diffractograms. In this aim the intensity in 2D images within "cake shape" sectors over the azimuth angle range equal to 15° degrees was integrated. Subsequently, the MULTIFIT program was used to determine diffraction peak position by fitting the peak profile with pseudo-Voigt function. The relative *elastic lattice strains* $< \varepsilon >_{\{hkl\}}$ (with respect to the initial inter-planar spacings) were calculated for different *hkl* reflections and for two orientations of the scattering vector:

$$< \varepsilon_{11} >_{\{hkl\}} = \frac{< d_{LD}^{\Sigma} >_{\{hkl\}} - < d_{LD}^{0} >_{\{hkl\}}}{< d_{LD}^{0} >_{\{hkl\}}} \text{ and } < \varepsilon_{22} >_{\{hkl\}} = \frac{< d_{TD}^{\Sigma} >_{\{hkl\}} - < d_{TD}^{0} >_{\{hkl\}}}{< d_{TD}^{0} >_{\{hkl\}}} \qquad (1)$$

where: $< d^{\Sigma} >_{\{hkl\}}$ and $< d^{0} >_{\{hkl\}}$ are the inter-planar spacings measured for the sample with and without external load, while the $< >_{\{hkl\}}$ brackets denote the average over the volume of diffracting grains for which the scattering vector is perpendicular to the {*hkl*} planes. Subscripts *LD* and *TD* indicates the directions of the inter-planar spacing measurement, i.e. along the direction of load and in transverse directions, respectively.
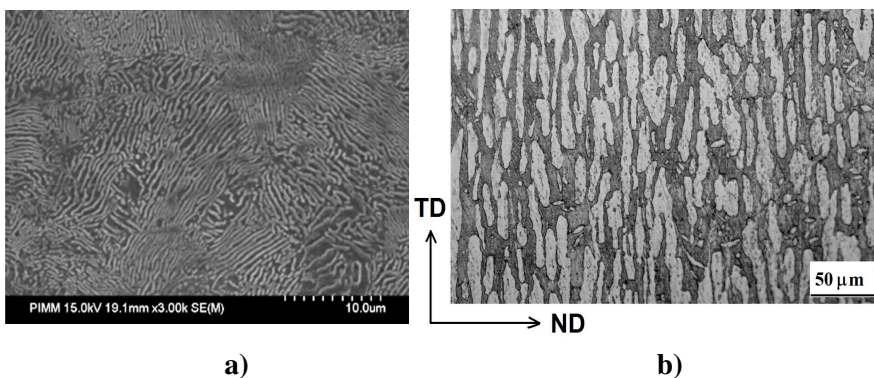

Fig. 1. Microstructure for: a) C70 pearlitic steel (scanning electron microscope), b) duplex steel (optical microscope: light islands of austenite in the dark ferrite matrix). The directions characteristic for rolling process are shown: RD-rolling, TD-transverse and ND-normal directions.

a)   b)

Table 1. Nominal chemical composition of the studied steels (wt%), Fe – balance.

	C	Mn	Cr	Ni	Mo	Cu	S	N	Si	P	Al
pearlitic steel EN C70	0.68	0.846	0.160	0.114	0.027	0.205	0.010	-	0.192	0.010	0.042
duplex stainless steel UR45N	0.015	1.6	22.4	5.4	2.9	0.12	0.001	0.17	-	-	-
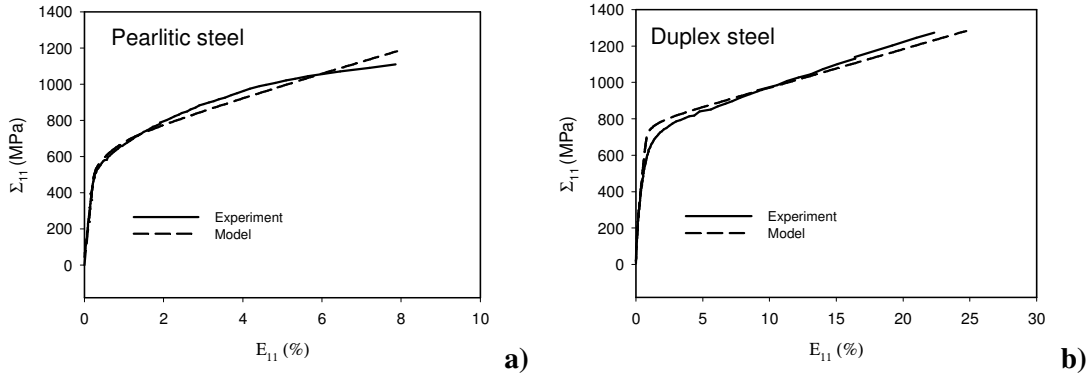
Fig. 2. Results of the mechanical tensile test performed during diffraction measurements (solid line) compared with model prediction (dashed line) for pearlitic (a) and duplex (b) steels.
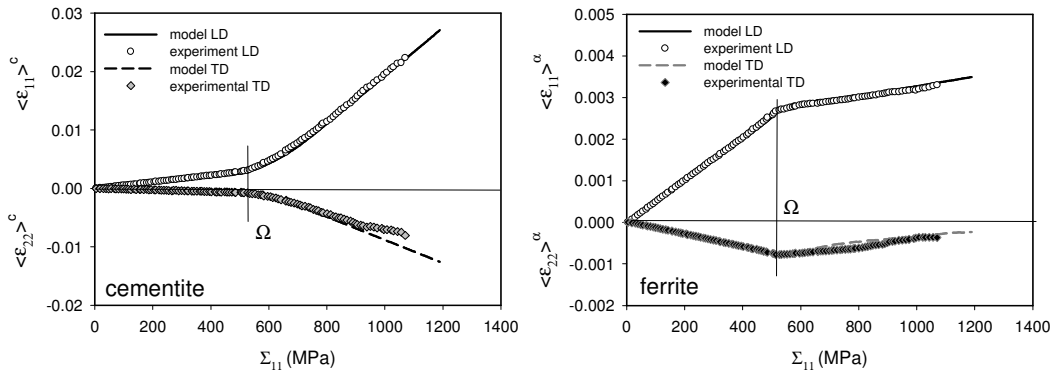
Fig. 3. The measured mean values of the elastic phase strains in pearlitic steel vs. applied stress. The experimental points determined in two directions (LD and TD) are compared with predicted lines for: a) cementite ($<\varepsilon_{11}>^c$ and $<\varepsilon_{22}>^c$) and b) ferrite ($<\varepsilon_{11}>^\alpha$ and $<\varepsilon_{22}>^\alpha$). Uncertainties are too small to be visible in the presented graphs.
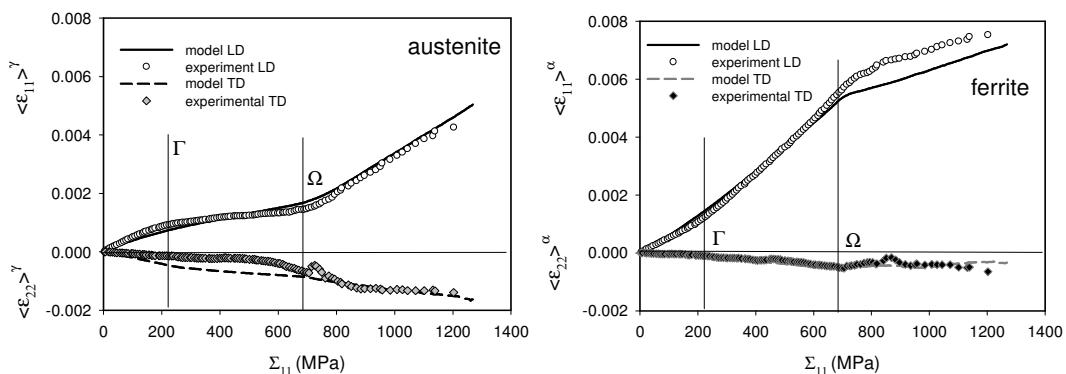
Fig. 4. The same comparison as in Fig. 3 but for duplex steel: a) austenite ($<\varepsilon_{11}>^\gamma$ and $<\varepsilon_{22}>^\gamma$) and b) ferrite ($<\varepsilon_{11}>^\alpha$ and $<\varepsilon_{22}>^\alpha$). Uncertainties are too small to be visible in the presented graphs.

Subsequently, the arithmetic averages $<\varepsilon_{11}>^{ph}$ and $<\varepsilon_{22}>^{ph}$, over all lattice strains $<\varepsilon_{11}>_{\{hkl\}}$ and $<\varepsilon_{22}>_{\{hkl\}}$ (see Eq. 1) measured in each *ph*-phase were calculated. As it was shown in [6] the $<\varepsilon_{11}>^{ph}$ and $<\varepsilon_{22}>^{ph}$ averages representatively describe elastic strains of the grains belonging to

the studied *ph*-phases. In the case of duplex steel average lattice strains ($ph = \gamma$) were calculated for reflections {111}, {200}, {220}, {331}, {400}, {222} in austenite and for {110}, {200}, {211}, {220}, {310} in ferrite ($ph = \alpha$). The same set of reflections was used for ferrite in the studied pearlitic steel, while the mean lattice strains in cementite ($ph = c$) were determined for {123}, {301}, {210} reflections. The average phase strains $<\varepsilon_{11}>^{ph}$ and $<\varepsilon_{22}>^{ph}$ in function of applied macrostress Σ_{11} are presented in Figs. 3 and 4.

Model prediction and discussion

The model calculations are performed at two different scales: the macro-scale, where the average quantities (Σ_{ij}, E_{ij}) are defined, and the grain-scale, on which the behaviour of each crystallite under local stress σ_{ij} is analyzed. At grain scale, plastic deformation occurs due to the slip on the crystallographic planes. According to Schmid's law, the slip can be activated only on a slip system s ≡ *[uvw] (hkl)* (the slip direction and slip plane are specified) for which the resolved shear stress reaches a critical value denoted by τ_c^s.

During plastic deformation, the multiplication of dislocations and the evolution of their spatial distribution inside a grain lead to the hardening of the slip systems (τ increases with deformation). In the kinetic description of the slip systems, their 'self' and 'latent' hardenings can be approximately described by a work hardening matrix [10] reflecting the interactions between the slip systems in the polycrystalline grain. The rate of critical shear resolved stress on the *s*-th system $\dot{\tau}_c^s$ is equal to:

$$\dot{\tau}_c^s = \sum_t H^{st} \dot{\gamma}^t \tag{2}$$

where $\dot{\gamma}^t$ is the rate of plastic glide in the *t*-th active system (dot means time derivative) , while H^{st} is the hardening matrix. In the present work the simplest isotropic and linear hardening was assumed, i.e., all components of hardening matrix are equal and independent on the sample strain: $H^{st} = H$.

In the elastoplastic deformation model, the above described processes should be considered at the grain scale. To this end, the scale transition theory can be used. This theory is based on the hypothesis of the existence of a concentration tensor A_{ijkl} (or B_{ijkl}) relating the overall macrostrain (or macrostress) rate $\dot{E}_{ij}$ (or $\dot{\Sigma}_{ij}$) with the grain strain (or stress) rate $\dot{\varepsilon}_{ij}$ (or $\dot{\sigma}_{ij}$) defined for a particular grain, i.e.:

$$\dot{\varepsilon}_{ij} = A_{ijkl} \dot{E}_{kl} \quad \text{and} \quad \dot{\sigma}_{ij} = B_{ijkl} \dot{\Sigma}_{kl} \tag{3}$$

In the present work, the algorithm given by Lipinski and Berveiller [11] was used for calculation of the localization tensors $A_{ijkl}^{(sc)}$ and $B_{ijkl}^{(sc)}$.

As will be seen in the sequel, in the case of the pearlitic steel, the prediction of self-consistent calculations does not agree with the experimental observations. These discrepancies were attributed to an incorrect prediction of the localization tensor $A_{ijkl}^{(sc)}$, when a high contrast exists between mechanical properties of the two phases. In this work the diffraction results are used to determine the localization tensor. To do this, it is assumed that the values of the actual localization tensor lie within the boundaries defined by the Taylor–Voigt assumption of homogenous strain (in this case $A_{ijkl}^{(TV)} = I_{ijkl}$, where I_{ijkl} is the unit four rank tensor) and by Sachs–Reuss assumption of homogenous stress (i.e., $B_{ijkl}^{(SR)} = I_{ijkl}$). The experimental results can then be compared with those calculated with localization tensors approximated by one of the following formulae:

$A_{ijkl} = \eta I_{ijkl} + (1-\eta)A_{ijkl}^{(sc)}$ - for localisation between self-consistent and Taylor–Voigt predictions (4a)

or

$B_{ijkl} = \varsigma I_{ijkl} + (1-\varsigma)B_{ijkl}^{(sc)}$ - for localisation between self-consistent and Sachs–Reuss predictions. (4b)

The adjustable parameters η and ς are determined comparing the theoretical data with experimental results.

To predict the elastoplastic process, the calculations were performed for 2000 spherical inclusions representing grains of austenite (50%) and ferrite (50%) in duplex steel, and grains of cementite (10% - calculated on the basis of carbon content) and ferrite (90%) in pearlitic steel. Tensile stress was applied along the rolling direction (RD). The initial orientations of crystallites corresponding to the experimental textures, and determined initial stresses were used as the input data for each phase of duplex steel [6]. Calculations were performed with the assumption that two families of slip systems (i.e. <111>{211} and <111>{110}) for ferrite and one family of slip systems (i.e. <110>{111}) for austenite are active during the plastic deformation. The elastic behaviour of austenitic and ferritic grains was characterized by given single crystal elastic constants [3,12] (see Table 2). The Young modulus and Poisson ratio for cementite were estimated from lattice strains measured during elastic deformation of the sample (Table 2).

The plastic properties of austenite and ferrite (τ and H, Eq. 2) were 'a priori' not known. The plastic deformation in each phase is described by different sets of parameters (τ and H) which can be determined through the comparing model and experimental data for macroscopic curves (Fig. 2) and mean lattice strains measured in both phases of the studied samples (Figs. 3 and 4).

In the case of pearlitic steel, yield point of ferrite can be identified due to significant change of trends in phase strains $<\varepsilon_{11}>^{ph}$ and $<\varepsilon_{22}>^{ph}$ evolution vs. applied stress occurring for both phases (approximate position of such change of trends is marked by Ω in Fig. 3). The slopes of the plots change because significantly higher load is transferred to cementite when plastic deformation in ferrite begins. By fitting self-consistent model to the experimental results the value of τ_c^s can be precisely estimated. To do this the position of the elastic-plastic transition in ferrite (indicated by Ω) must be adjusted varying τ_c^s value in model calculation [4,6]. It was found that above the Ω threshold the self-consistent model did not correctly predict partitioning of the stresses between phases, therefore the localization was modified using Eqs. 4. An excellent agreement of the experimental and theoretical lattice strains was found (Fig. 3) if the localization tensor for cementite was set between self-consistent and Taylor-Voigt models: $A_{ijkl} = 0.75 \cdot A_{ijkl}^{(sc)} + 0.25 \cdot I_{ijkl}$ (i.e., $\eta = 0.25$ in Eq. 4a). The best fit of all plots (Fig. 2a and Fig. 3) was obtained for the parameters given in Table 2. No significant changes in the trends of the measured lattice strains vs. applied stress were observed after Ω threshold (Fig.3). Only small deviation of experimental $<\varepsilon_{22}>^c$ strains from the model values is observed in cementite over Σ_{11}= 900 MPa, but the other plots ($<\varepsilon_{11}>^a$ and $<\varepsilon_{22}>^a$ in ferrite and $<\varepsilon_{11}>^c$ in cementite) agree very well with the theoretical results obtained assuming elastic deformation of cementite and plastic deformation of ferrite. It means that plasticity occurs in the ferritic phase, while most of the cementite grains remain elastic for the whole range of deformation (small deviation of $<\varepsilon_{22}>^c$ strains in cementite from the model can be explained due to plasticity or damage occurring for cementite grains having specific orientations).

Analyzing the lattice strain vs. applied stress it can be found that elastic range in both phases of duplex steel occurs up to Γ threshold, where plastic deformation of austenitic phase begins and much higher load is transferred to ferrite (Fig. 4). After this threshold a high stress localized in still elastic ferrite and low stresses in plastically deformed austenite was observed. Next, at the limit Ω ferritic grains start to yield and the partition of the phase stresses changes again. Above Ω threshold slightly slower increase of the loading occurs for ferrite in comparison with austenite (hardening process is more significant in austenitic phase). Small instabilities seen on the experimental plots

occurred probably due to heterogeneity/anisotropy of plastic deformation for different groups of polycrystalline grains. The values of critical resolved shear stresses (τ_c^s) as well the hardening parameters (*H*) were found (Table 2), adjusting model calculations to the experimental results (Figs. 2b and 4). In the case of duplex steel the localization is well predicted by self-consistent approach (i.e. $A_{ijkl} = A_{ijkl}^{(sc)}$).

Table 2. Elastic constants for grains of ferrite [3,12] and cementite (adjusted for elastic range of deformation); and parameters of plastic deformation determined in tensile test for ferritic and austenitic phases.

Material	Phase	c_{11} (GPa)	c_{12} (GPa)	c_{44} (GPa)	τ_c^s (MPa)	H (MPa)
Pearlitic steel EN C70	Cementite	E= 175 GPa and ν=0.275			-	-
	Ferrite	231	134	116	220	100
Duplex stainless steel UR45N	Austenite	198	125	122	140	260
	Ferrite	231	134	116	450	130

Summary

High energy diffraction during tensile test and elastoplastic models were used to study pearlitic and duplex steels. The stress partition between two phases was successfully determined for both materials. In the case of pearlite only the ferritic phase is plastically deformed, while the cementite remains elastic. In duplex steel both phases undergo plastic deformation, but the yield stress of ferrite is higher than the yield stress of austenite. The critical resolved shear stress (τ_c^s) and work hardening parameter (*H*) were determined for plastically deformed phases in both materials. Finally it was found that the strain rate localization on polycrystalline grains is well predicted by self-consistent model for duplex steel, however the strain localization in the grains of cementite is between self-consistent and Taylor-Voigt models. This leads to higher value of stress in cementite comparing with that predicted by self-consistent approach. To find out the reason of the intermediate type of stress localisation (between two models) the mechanical coupling between ferritic and cementite grains is currently studied.

References

[1] B. Clausen, T. Lorentzen, M.A.M. Bourke, M.R., Daymond, Mater. Sci. Eng. A 259 (1999) 17–24.

[2] S. Cai, M.R. Daymond, R.A. Holt, Acta Mater. 57 (2009) 407–419.

[3] K. Inal, P. Gergaud, M. Francois & J.-P. Lebrun (1999). Scand. J. Metall. 28, 139–150.

[4] A. Baczmański and C. Braham, Acta Mater. 59 (2004) 1133-1142.

[5] R. Dakhlaoui C. Braham, A. Baczmański, Mat. Sci. Eng. (A), 444 (2007) 6-17.

[6] A. Baczmanski , L. Le Joncour, B. Panicaud, M. Francois, C. Braham, A.M. Paradowska. S. Wroński, S. Amara and R. Chiron, J. Appl. Cryst. 44 (2011) 966-982.

[7] J.E. Daniels & M.J. Drakopoulos, J., Synchrotron Rad.16 (2009) 463-468.

[8] A.P. Hammersley, S.O. Svensson, M. Hanfland, A.N. Fitch and D. Häusermann, High Pressure Research, 14 (1996), 235-248,

[9] S. Merkel, Multifit/ Polydefix Polycrystal Deformation using X-rays, *https://code.google.com/p/multifit-polydefix/*

[10] P. Franciosi , M. Berveiller, Acta Met. 28 (1980) 273-283.

[11] P. Lipinski and M. Berveiller, Int. J. Plast. 5 (1989) 149–172.

[12] G. Simoms & H. Wang, H. (1971). Single Crystal Elastic Constants and Calculated Aggregate Properties: A Handbook, 2nd ed. Cambridge,London: The MIT Press.